

50. Internationales Wissenschaftliches Kolloquium

September, 19-23, 2005

**Maschinenbau
von Makro bis Nano /
Mechanical Engineering
from Macro to Nano**

Proceedings

Fakultät für Maschinenbau /
Faculty of Mechanical Engineering

Startseite / Index:

<http://www.db-thueringen.de/servlets/DocumentServlet?id=15745>

Impressum

- Herausgeber: Der Rektor der Technischen Universität Ilmenau
Univ.-Prof. Dr. rer. nat. habil. Peter Scharff
- Redaktion: Referat Marketing und Studentische Angelegenheiten
Andrea Schneider
- Fakultät für Maschinenbau
Univ.-Prof. Dr.-Ing. habil. Peter Kurtz,
Univ.-Prof. Dipl.-Ing. Dr. med. (habil.) Hartmut Witte,
Univ.-Prof. Dr.-Ing. habil. Gerhard Linß,
Dr.-Ing. Beate Schlütter, Dipl.-Biol. Danja Voges,
Dipl.-Ing. Jörg Mämpel, Dipl.-Ing. Susanne Töpfer,
Dipl.-Ing. Silke Stauche
- Redaktionsschluss: 31. August 2005
(CD-Rom-Ausgabe)
- Technische Realisierung: Institut für Medientechnik an der TU Ilmenau
(CD-Rom-Ausgabe) Dipl.-Ing. Christian Weigel
Dipl.-Ing. Helge Drumm
Dipl.-Ing. Marco Albrecht
- Technische Realisierung: Universitätsbibliothek Ilmenau
(Online-Ausgabe) [ilmedia](#)
Postfach 10 05 65
98684 Ilmenau
- Verlag:  Verlag ISLE, Betriebsstätte des ISLE e.V.
Werner-von-Siemens-Str. 16
98693 Ilmenau

© Technische Universität Ilmenau (Thür.) 2005

Diese Publikationen und alle in ihr enthaltenen Beiträge und Abbildungen sind urheberrechtlich geschützt.

ISBN (Druckausgabe): 3-932633-98-9 (978-3-932633-98-0)
ISBN (CD-Rom-Ausgabe): 3-932633-99-7 (978-3-932633-99-7)

Startseite / Index:

<http://www.db-thueringen.de/servlets/DocumentServlet?id=15745>

Model Building, Control Design and practical Implementation of a MEMS Acceleration Sensor

Heiko Wolfram, Ralf Schmiedel, Torsten Aurich, Jan Mehner, Thomas Geßner and
Wolfram Dötzel

ABSTRACT

This paper presents some new results on MEMS acceleration sensors. An approximate method is described to analytically analyze deep airstream channels on the mass surface. The channels enormously decrease the squeeze-film damping force for ambient pressure inside the sensor. The ambient pressure simplifies the fabrication process and guarantees approximate equal dynamics for all sensor samples. The sensor fabrication and design is shortly covered. A theoretical model is built from the physical principles of the complete sensor system, consisting of the MEMS sensor, the charge amplifier and the PWM driver for the sensor element. A reduced-order model of the entire system is used to design a robust control with the \mathcal{H}_∞ -Approach. The weighting takes the plant-input disturbance into account and prevents a slow disturbance rejection, which is the case for the S/KS-design. Remarks are given on the identification of the mechanical system. Practical tests and the system identification prove the newly found results.

Keywords: Acceleration Sensor, Model Building, \mathcal{H}_∞ -Control, Mixed-Sensitivity Approach, Identification

1. INTRODUCTION

MICRO-ELECTRO-MECHANICAL systems (MEMS) play an important role in the realization of sensor/actuator systems. They are small, very compact, have a simple and robust layout. Another advantage is the technology, which can directly be applied from the micro electronics and hence, makes the integration of the electronics and the production of large quantities possible. There are, however, some limitations such as packaging, cross-talk related problems, the MEMS mechanical limitation. A major problem for the control design and stability is the strong nonlinearity of the electrostatic field component and the nonlinearity of fluid damping. Therefore, an intensive analysis of the open and closed-loop system may be necessary.

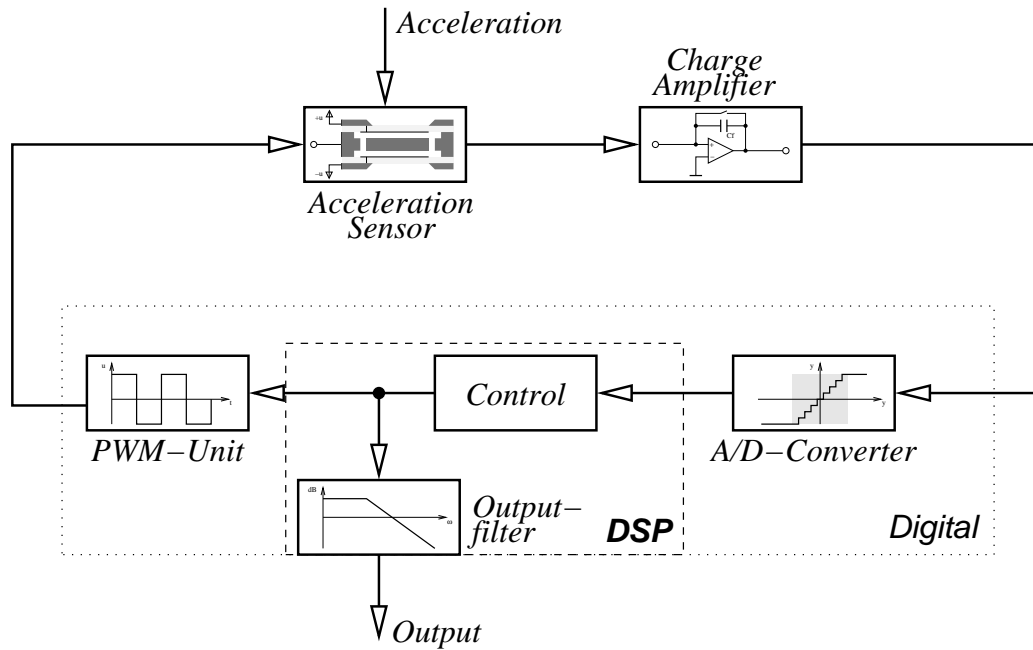


Figure 1. Block diagram of the system

Control systems were widely applied to MEMS to improve the system behavior. A sigma-delta converter [1, 2] was used to control an accelerometer. A phase lead-lag controller in combination with a second-order low-pass filter [3] was successfully attached to micro-mirror systems. A Kalman observer based state feedback with integral action [4] as well as further control schemes like PD and phase-lead control [5] found its application for micro-actuators.

Nonlinear control, such as model-reference adaptive control systems (MRAC) were successfully applied to micro-mirrors [6] and gyroscopes [7, 8], as well as a model-reference based neural network (NN) [9] on an accelerometer. Sliding-mode control [10] and PID control with non-linearity inversion and gain-scheduling [11] was used to control micro-mirrors.

From control theory is known, that special requirements are needed or limitations exist. The sigma-delta converter is a proportional control with limited tuning possibilities, the tuning rule for the phase lead-lag, PD controller rely on practical tests and the pole-placement control needs full state measurement or generation.

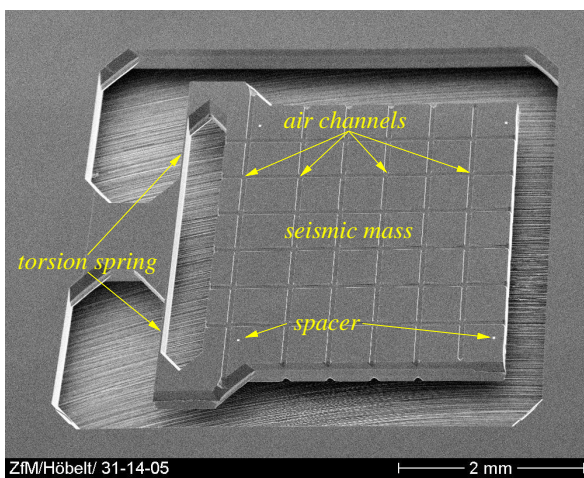
There are, however, limitations for the nonlinear approaches – MRAC cannot be applied to non-minimum phase systems and might be impractical for fast time-varying systems. Similarly, gain-scheduling assumes a slow altering scheduling variable and the scheduling variable should capture the

plant nonlinearities. The non-linearity inversion assumes a perfect cancellation and the sliding-mode control produces high-frequency switching in the control-loop. Further, the NN approach just gives a black-box model with no knowledge of the inside dynamical system and needs a large amount of training data sets.

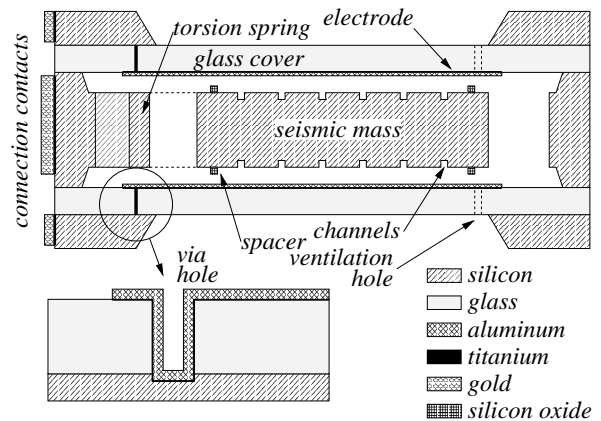
All applied control schemes are developed in time domain and except of the MARC, sliding-mode control and gain-scheduling do not consider robustness explicitly. Therefore, the \mathcal{H}_∞ control design is introduced to control the system, depicted in Fig. 1. Since there is no guaranteed stability for the developed linear time-invariant (LTI) control on the nonlinear system, stability analysis has to be given explicitly. This will be a task for the future.

2. DESIGN

A capacitance acceleration sensor has been developed in bulk micro machining technology. It consists of a silicon wafer with the mechanical structure (Fig. 2(a)) and glass wafers with the electrodes, which are anodic bonded to both sides of the silicon wafer. Fig. 2(b) shows the sensor's schematic configuration.



(a) SEM micrography of the seismic mass



(b) Schematic configuration

Figure 2. The sensor chip

By using silicon-nitride and silicon-oxide as mask layers, eight different masks (four for each side) are used to etch the spring-mass components into the silicon wafer (Fig. 3). Caps of about $3 \mu\text{m}$ are

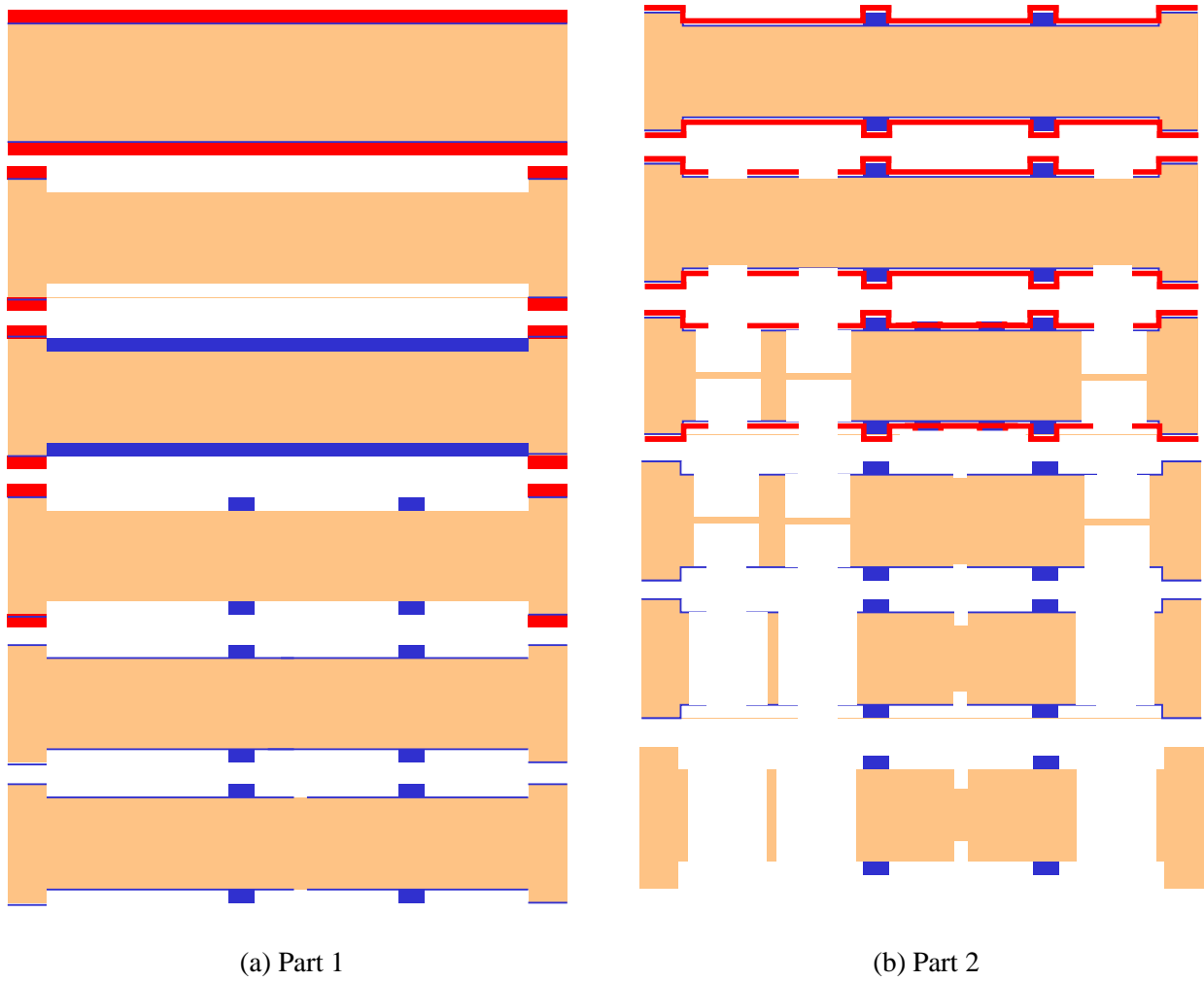


Figure 3. Process steps

wet etched in KOH-solution with the first masks (front and back side). A following LOCOS-process is used to grow up $1\ \mu\text{m}$ thermal oxide on the mass-surface. The second masks structure the oxide to create oxide spacers on the surface of the mass. These spacers prevent the electrical contact between mass and electrodes and also the sticking during the bonding process. The third masks are used to etch $30\ \mu\text{m}$ deep channels into the mass to minimize the squeeze-film effect. Finally the spring-mass components are etched into silicon. All masks are designed to create components, which are rotated with an angle of 45° in relation to wafer flat. The under-etching rate is nearly the same as the deep-etch rate. That means, that the cross-section of the springs has a rectangular shape.

Silicon wafers were anodic bonded on the glass wafers and structured to get silicon islands. Holes

are ultrasonic drilled into the glass wafers to get the electrical contact from outside to inside of the glass wafers and the equalization to ambient pressure. The holes have a diameter of 500 μm and a deepness of about 600 μm . Silicon hard-masks are used to sputter aluminum electrodes and to realize the connection between electrodes and outer silicon islands.

One silicon wafer is anodic bonded together with two glass wafers to get the final sensor. The process parameters are a temperature of 400 °C, ambient pressure and a voltage of 300 V. The ambient pressure guarantees equal heating of silicon and glass wafers during bonding process, and thus minimizes the deformation of the components after cooling down. An electric charge on top of the SiO₂-spacers can emerge from the anodic bonding process, which can create an additional unknown electrostatic moment. The outer islands are connected with the middle wafer during the bonding process to prevent this effect. A bonding grid at the outside of the glass wafers applies the bonding voltage exactly to the position of the silicon frame on the silicon wafer.

The sensors are separated and a final sputter process supplies the side wall contacts. Therefore, some sensors are put together in a sputter feature and covered by a hard-mask to separate the connection contacts. Bonding wires finally connect the sensor to the electronics.

3. MODEL BUILDING

The acceleration sensor can generally be described as a spring-mass system

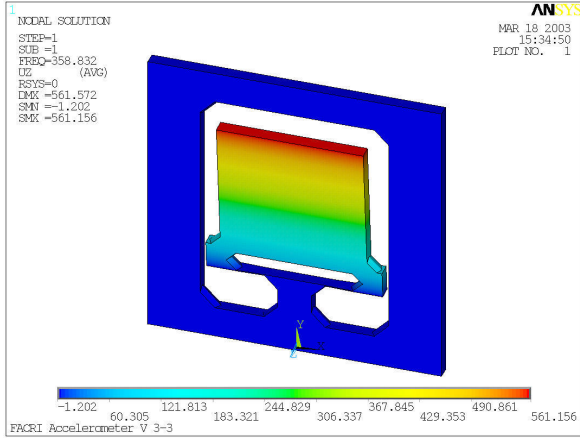
$$[-\omega^2 \mathbf{M} + j\omega\{\mathbf{D} + \mathbf{D}_s(\omega, \mathbf{v}(\omega))\} + \mathbf{K} + \mathbf{K}_s(\omega, \mathbf{v}(\omega))] \mathbf{v}(\omega) = \mathbf{p}_{ext}(\omega) + \mathbf{p}_{el}(\mathbf{v}(\omega), u(\omega)) \quad (1)$$

with the inertial matrix \mathbf{M} , the damping matrix \mathbf{D} and stiffness matrix \mathbf{K} , consisting of constant mechanical and frequency dependent squeeze-film parts, the displacement vector \mathbf{v} and the load vectors, the electrostatic load \mathbf{p}_{el} and the disturbance, the mechanical load \mathbf{p}_{ext} .

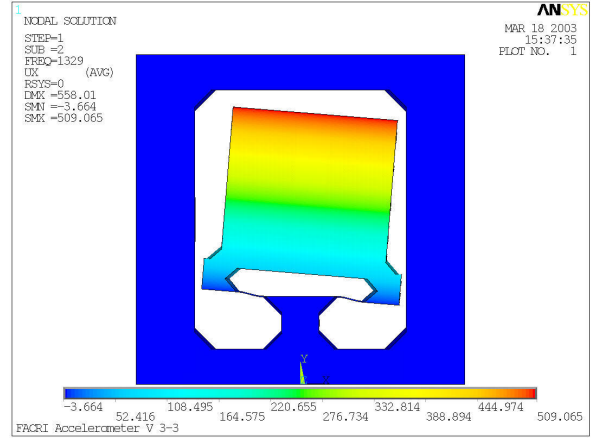
The mechanical system has in general several degrees of freedom, where only the first mode

$$f_0 = \frac{1}{2\pi} \sqrt{\frac{K}{J}} \quad (2)$$

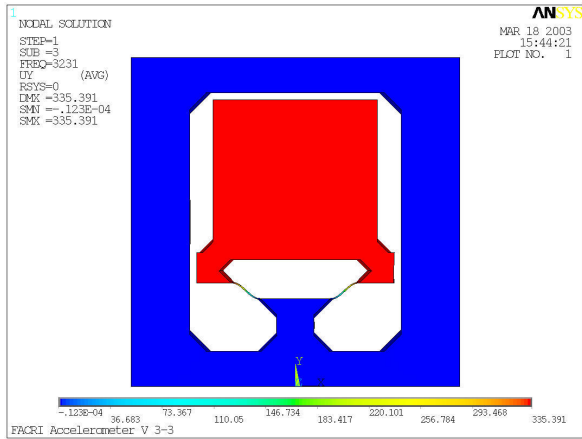
with the moment of inertia J and mechanical spring constant K is considered. The higher degrees of freedom usually appear in higher frequency areas (Fig. 4), which are uncontrollable and undetectable from the electronics.



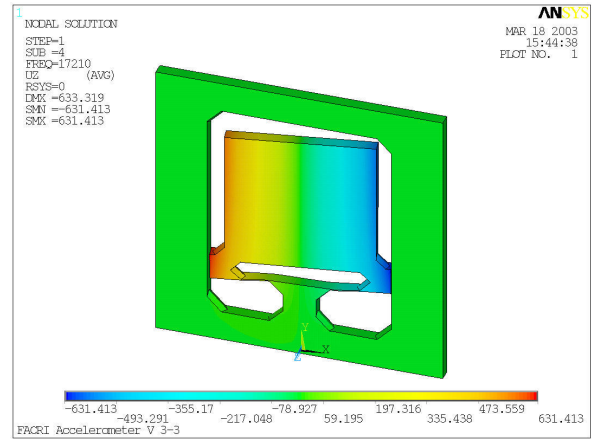
(a) First mode $f_0 = 359$ Hz



(b) Second mode $f_0 = 1329$ Hz



(c) Third mode $f_0 = 3229$ Hz



(d) Fourth mode $f_0 = 17$ kHz

Figure 4. First four results of the modal analysis

The mechanical constants can be derived from the mechanical laws, where the mass has the dimension $a_m \times b_m \times d_m$ (width \times length \times thickness) and the beam the dimension $a_b \times b_b \times d_b$. The calculation of the spring constant further needs the elastic shear modulus of silicon G and the torsion moment of inertia for a rectangular profile I_t

$$I_t = \frac{1}{3} \left(1 - \frac{0.630}{n} + \frac{0.052}{n^5} \right) a_b^3 d_b, \quad n = \frac{d_b}{a_b} \geq 1, \quad (3)$$

which can be found in [12].

| mechanical | | electrical |
|----------------------|-------------------------------------|--------------------------------|
| translatory | rotatory | |
| mass M | moment of inertia J | capacitance C |
| spring constant K | spring constant K | inverse inductance L^{-1} |
| damping constant D | damping constant D | conductance $G = R^{-1}$ |
| velocity $v(t)$ | angular velocity $\dot{\varphi}(t)$ | voltage $u(t) = \dot{\phi}(t)$ |
| force $F(t)$ | Moment $M(t)$ | current $i(t)$ |
| displacement $x(t)$ | angle $\varphi(t)$ | magnetic flow |
| | | $\phi(t) = Li_L(t)$ |

Table 1. Force-current analogy and its relation between mechanical and electrical components

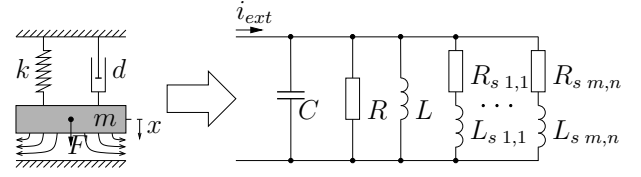


Figure 5. Analogy model of a spring mass system

3.1. Squeeze-Film Effect

Fluid damping generally plays an important role in micro systems, because of very small distances between moving parts. The fabricated acceleration sensor works at ambient pressure and therefore uses the gas in the gap as the damping element. Because of the compressibility of air, the gas produces frequency dependent damping and spring parts, where the damping part decreases and spring part increases with growing frequency.

The desired frequency response can be controlled with a proper gas pressure. In our case, the frequency behavior can be further achieved with changing the depth, width and amount of the airstream channels on the mass surface.

General flow problems can be described with the *Navier-Stokes Equations*. A special simplification, the *Reynolds Lubrication Equation* [13], describes the pressure distribution in a small air gap between two moving plates. A simple, linear dependence can be derived with a Taylor approximation and further neglecting high order terms. The resulting differential equation can be solved with separating the variables, which was done in [14] for parallel moving rectangular plates. The procedure was extended in [15] to tilting rectangular plates with a variational rotation axis. With using the force-current analogy, which is summarized in Tab. 1, the result alters to an infinite sum of series connections of a resistance and inductance (Fig. 5). A new variable, the squeeze number

$$\sigma = \frac{12\mu a^2}{p_0 d_0^2} \quad , \quad (4)$$

was introduced in [14] for solving the linearized differential equation. The gauges a and b denote the width and length of the plate, p_0 the nominal pressure, d_0 the nominal gap width and μ the viscosity. An one-term approximation of the squeeze-film damping parts is sufficiently accurate for most practical purposes [14]. Tab. 2 summarizes the squeeze-film damping results for both, the translatory and

rotatory motion.

REMARK 1. *An analytical solution of the plate with airstream channels is not a trivial task. The channels are deep enough to set the pressure inside of them to nominal pressure. This approximation would split of the plate area into $(n_x + 1)(n_y + 1)$ small planes with the new dimension*

$$\tilde{a} = \frac{a - n_x w_g}{n_x + 1} \quad \text{and} \quad \tilde{b} = \frac{b - n_y w_g}{n_y + 1} \quad , \quad (5)$$

where w_g is the width of the channels, n_x the number in x -direction and n_y in y -direction. The summation of all spring and damping forces gives the resulting load

$$\tilde{R}_{s\ m,n}^{tran} = \frac{1}{(n_x + 1)(n_y + 1)} R_{s\ m,n}^{tran} \quad \text{and} \quad \tilde{L}_{s\ m,n}^{tran} = \frac{1}{(n_x + 1)(n_y + 1)} L_{s\ m,n}^{tran} \quad , \quad (6)$$

which is valid for the translatory movement.

The rotatory motion needs some more calculation, since the rotation axis varies from plane to plane. One gets the solution of the squeeze-film parts for a variational rotation axis [15]

$$R_{s\ 1,1}^{rot} = \frac{d_0 \pi^6}{64 a^3 b \zeta^2 p_0 \sigma} \left(1 + \frac{a^2}{b^2} \right) \quad \text{and} \quad L_{s\ 1,1}^{rot} = \frac{d_0 \pi^4}{64 a^3 b \zeta^2 p_0} \quad . \quad (7)$$

A one-term approximation is in this case correct, since the distance $\zeta = c/a$ will be a factor of $1/2$. The length c defines the distance of the rotation axis to the barycentric axis of each plane. A summation of all moments gives

$$\tilde{R}_{s\ 1,1}^{rot} = \frac{\zeta^2}{(n_y + 1) \tilde{\zeta}^2} R_{s\ 1,1}^{rot} \quad \text{and} \quad \tilde{L}_{s\ 1,1}^{rot} = \frac{\zeta^2}{(n_y + 1) \tilde{\zeta}^2} L_{s\ 1,1}^{rot} \quad (8)$$

where

$$\tilde{\zeta}^2 = \sum_{n=0}^{n_x} \frac{(2n + 1)^2}{4} = \frac{(1 + n_x)(1 + 2n_x)(3 + 2n_x)}{12} \quad . \quad (9)$$

The gap between each plate can be neglected for the moment calculation, as long as $\tilde{a} \gg w_g$. For the approximation is further supposed, that the channel depth is greater than the mean free path $d_g \gg d_0$ and the plate area $\tilde{a} \times \tilde{b}$ not too small.

A detailed analysis of airstream channels can be found in [16], which considers the actual pressure distribution and the viscous friction on the sidewalls.

The transfer function of the acceleration sensor can be easily get from the state-space description, found from the *Kirchhoff Equations*. An one-term approximation for the squeeze-film parts at the top and bottom side is sufficiently accurate, since the seismic mass is controlled in zero position. The model for the control design reduces further to

$$G_{mech} = \left[\begin{array}{c|c} \mathbf{A} & \mathbf{B} \\ \hline \mathbf{C} & \mathbf{D} \end{array} \right] = \left[\begin{array}{ccc|c} -\frac{1}{CR} & -\frac{1}{C} & -\frac{1}{C} & \frac{1}{C} \\ L^{-1} & 0 & 0 & 0 \\ L_s^{-1} & 0 & -\frac{R_s}{L_s} & 0 \\ \hline 0 & L & 0 & 0 \end{array} \right] \quad \text{with the values} \quad \begin{array}{l} R_s = \frac{1}{2}R_{s\ 1,1} \\ L_s = \frac{1}{2}L_{s\ 1,1} \end{array} \quad (10)$$

This approximation will be also used for the control design, since the order of the model directly determines the order of the controller.

3.2. LTI System Model

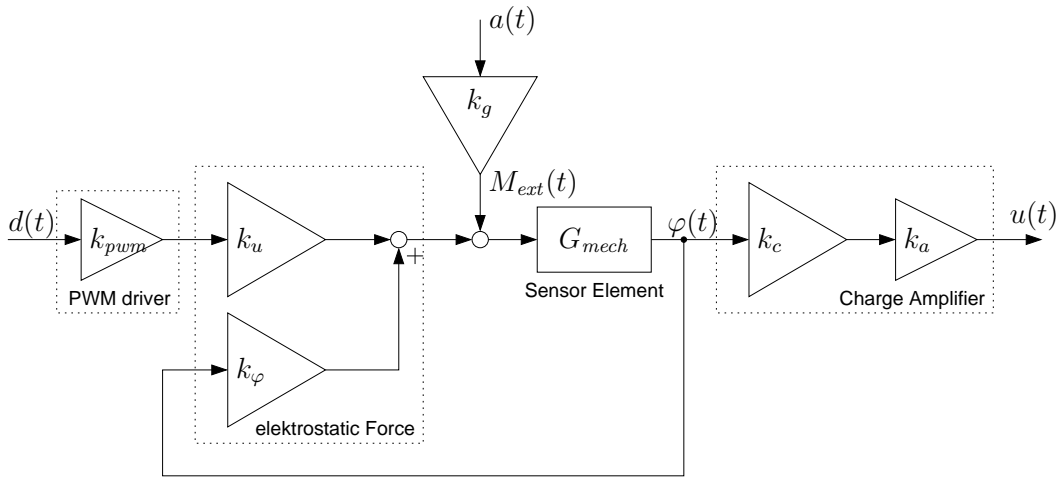


Figure 6. LTI system model

The LTI model of the complete system shows Fig. 6. The system contains an inner loop part with positive feedback, which is responsible for the system instability, known as spring-softening effect. The other gains rise the open-loop gain of the system. The plant model for the control design results into

$$\dot{\mathbf{x}} = (\mathbf{A} + k_\varphi \mathbf{B}\mathbf{C}) \mathbf{x} + \mathbf{B}k_u k_{pwm} \mathbf{u}, \quad \mathbf{y} = k_a k_c \mathbf{C}\mathbf{x} \quad (11)$$

Tab. 2 summarizes all needed gains for calculation, where the derivation can be found in [15].

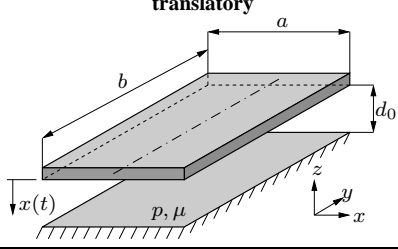
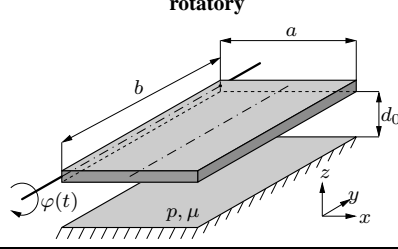
| | translatory | rotatory |
|-------------------------|----------------------------------------------------------------------------------------------------------------------------------------------------------------------------------------------------------|--------------------------------------------------------------------------------------------------------------------------------------------------------------------------------------------------------------------------------------------|
| |  |  |
| Mechan. parameters | $m = \rho_S a_m b_m d_m, \quad K$ | $J = \frac{1}{12} m (a_m^2 + d_m^2 + 12c^2), \quad K = 2 \frac{GI_t}{b_b}$ |
| First eigenfrequency | $f_0 = \frac{1}{2\pi} \sqrt{\frac{K}{m}}$ | $f_0 = \frac{1}{2\pi} \sqrt{\frac{K}{J}}$ |
| Charge amplifier | $k_a = -\frac{u_b}{C_f}$ | |
| Detection sensitivity | $k_c = -\frac{2\varepsilon ab}{d_0^2}$ | $k_c = -\frac{\varepsilon a^2 b}{d_0^2}$ |
| PWM driver | $k_{pwm} = u_b$ | |
| Kinetic actuation | $k_g = m$ | $k_g = \frac{ma}{2}$ |
| Electrostatic actuation | $k_x = \frac{\varepsilon ab}{2d_0^3} (4u^2 + u_b^2)$ $k_u = \frac{\varepsilon abu_b}{d_0^2}$ | $k_\varphi = \frac{\varepsilon a^3 b}{6d_0^3} (4u^2 + u_b^2)$ $k_u = \frac{\varepsilon a^2 bu_b}{2d_0^2}$ |
| Squeeze-film parts | $L_{s\ m,n}^{tran} = \frac{m^2 n^2 d_0 \pi^4}{64abp_0}; \quad m, n \in \{1, 3, 5, 7, \dots\}$ $R_{s\ m,n}^{tran} = \frac{m^2 n^2 d_0 \pi^6}{64abp_0 \sigma} \left(n^2 + \frac{a^2 m^2}{b^2} \right)$ | $L_{s\ m,n}^{rot} = \frac{m^2 n^2 d_0 \pi^4}{16a^3 bp_0} \quad m \in \{1, 3, 5, 7, \dots\},$ $n \in \{1, 2, 3, 4, \dots\}$ $R_{s\ m,n}^{rot} = \frac{m^2 n^2 d_0 \pi^6}{16a^3 bp_0 \sigma} \left(n^2 + \frac{a^2 m^2}{b^2} \right)$ |

Table 2. Summary of the system gains at zero position

4. IDENTIFICATION

The identification of the mechanical system is not a trivial task. First, a known acceleration must be applied to the sensor and the seismic mass has to be observed with an optical instrumentation. This could be a very costly job and might be even impossible for an opaque system.

An alternative to circumvent this problem is to use the electrostatic system and to calculate back the underlying mechanical system. This can be done with a two-stage identification [17], which identifies the system at an operating voltage near zero. The dynamics of the electrostatic system is in that stage close to the mechanical system behavior. The mechanical system DC gain is got from the measured resonance frequency of the spring-mass system in the unmounted stage. The second stage fine-tunes the system at nominal operating voltage.

A better alternative to identify the mechanical system, including the system gains, can be found in [15]. The identification uses the voltage dependences of the linearized gains and interpolates them with a polynomial. This means, that only two identifications at different operating voltages are needed to completely calculate back the mechanical system. The algorithm was stated as following:

ALGORITHM 1. *The pole movement under varying operating voltage can be approximately described with a parabola of second order around the zero operating voltage*

$$p_{j_{el}}(u_b) \approx (\varphi_{j_{0r}} + \varphi_{j_{2r}}u_b^2) + j(\varphi_{j_{0i}} + \varphi_{j_{2i}}u_b^2) \quad , \quad (12)$$

where the vertex of the parabola defines the approximate pole location of the mechanical poles $\varphi_{j_{0r}} + j\varphi_{j_{0i}}$.

The value of the mechanical plant gain k_p can be approximately calculated from the dominant real pole to

$$k_p \approx \frac{\varphi_{1_{2r}}u_b^2}{k_\varphi(u_b)} \quad . \quad (13)$$

The system forward gain $k_p\hat{k}$ is the static gain of the electromechanical System G_{emech} divided by the quotient of the products of the pole and zero locations

$$k_p\hat{k} = G_{emech}(s=0, u_b) \frac{\prod_{j=1}^n -p_{j_{el}}(u_b)}{\prod_{i=1}^m -z_i} \quad , \quad (14)$$

where $G_{emech}(s)$ is a strictly proper system ($n > m$).

The dependence of the gain $k_p\hat{k}$, where $\hat{k} = k_u(u_b)k_a(u_b)k_c k_{pwm}(u_b)$ is described with a cubic parabola in u_b

$$k_p\hat{k} = \varphi_3 u_b^3 \quad . \quad (15)$$

REMARK 2. A similar estimation of the plant gain as in Eq. (13) could be also get for the two dominant imaginary poles

$$k_p \approx \frac{\varphi_{20i}^2 - (\varphi_{22i} u_b^2)^2}{k_\varphi(u_b)} \quad (16)$$

of an undamped system.

The Identification algorithm relies on the exactly known order m and n . Subspace Identification [18] directly determines the system order n from the input-output data. The transformation rule $z = e^{sT_s}$ can be easily applied to the poles and a mean value of the zeros \bar{z}_i can be used to calculate back the system gain in Eq. (14).

It is clear, that the identification routines just only consider the small-signal model at the equilibrium point. Therefore, a very low excitation signal is only appropriate.

NOTE 1. Finding the system zeros in S -domain is not a trivial task. Identification routines generally find a discrete-time system model. The Z -Transformation might increase the numerator order and the location of the zeros vary with the location of the poles. A simple example

$$G(s) = \frac{1}{(s + p_1)(s + p_2)} \quad \overset{z}{\circ} \bullet \quad G(z) = \frac{p_1(1 - e^{-T_s p_2})(z - e^{-T_s p_1}) - p_2(1 - e^{-T_s p_1})(z - e^{-T_s p_2})}{p_1 p_2 (p_1 - p_2)(z - e^{-T_s p_1})(z - e^{-T_s p_2})} \quad (17)$$

shows the problem of the transformation. A sign of order discrepancy in the identification are very fast poles and zeros, which should be canceled.

5. CONTROL DESIGN

The S/KS/GS/T-Standard-Design Problem is used for the control design. In this design, the transfer function matrix \mathbf{N} will be minimized with the ∞ -Norm.

$$\mathbf{N}(\mathbf{K}) = \begin{bmatrix} \mathbf{W}_e \mathbf{S} \mathbf{W}_w & -\mathbf{W}_e \mathbf{S} \mathbf{G} \mathbf{W}_d \\ \mathbf{W}_u \mathbf{K} \mathbf{S} \mathbf{W}_w & -\mathbf{W}_u \mathbf{T}_i \mathbf{W}_d \\ \mathbf{W}_y \mathbf{T} \mathbf{W}_w & \mathbf{W}_y \mathbf{S} \mathbf{G} \mathbf{W}_d \end{bmatrix} \quad (18)$$

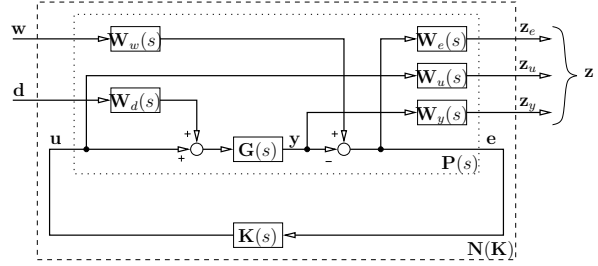


Figure 7. Block description of the S/KS/GS/T standard problem

The \mathcal{H}_∞ problem is the minimization of the transfer function matrix \mathbf{N}

$$\min_{\mathbf{K}} \|\mathbf{N}(\mathbf{K})\|_\infty$$

over all stable and proper controllers \mathbf{K} [19]. Fig. 7 depicts the general control loop, where y is the plant output, w the reference signal, u the control signal, d the plant input disturbance, e the error signal and z the performance signals, which are object for minimization.

The main objective is in our case the loop-shaping of the complementary sensitivity transfer function $\mathbf{T}_i = \mathbf{K} \mathbf{G} [\mathbf{I} + \mathbf{K} \mathbf{G}]^{-1}$. Thus, the command response will be optimized. A constant bound is further put on the control signal to avoid actuator saturation. Additional bounds are added on w and e to ensure, that the controller is proper. The realization of the weighting scheme is done with proper weighting factors \mathbf{W}_x at the inputs and outputs of the block $\mathbf{P}(s)$.

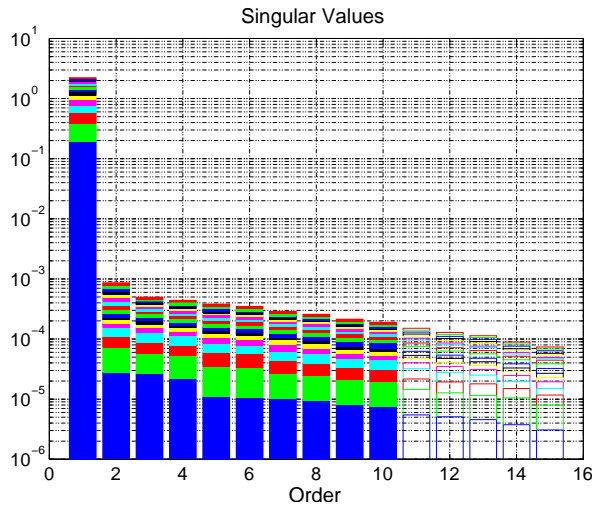
6. RESULTS

The identification and control design routine have been successfully applied to several samples. Fig. 8(a) shows the singular values from the subspace identification of the identified system, where the operating voltage u_b is varied. It can be seen, that a simple first-order system is sufficiently accurate for identification. The mechanical model*

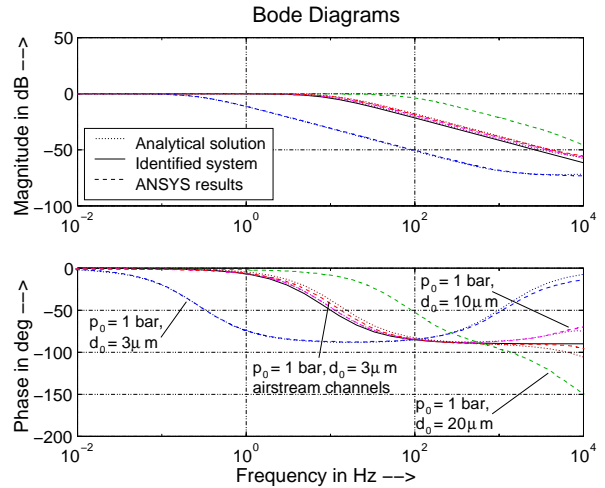
$$G_{mech} = \frac{0.2249}{s + 52.63}; \quad k_{corr} = 0.45 \quad (19)$$

is evaluated from the identification algorithm, where k_{corr} indicates the correction gain in the outer loop.

*The translatory approach has been used for reasons of simplicity and numerical computation.



(a) Singular values from the subspace identification



(b) Evaluated models compared to identified model

Figure 8. Results from identification and simulation

Fig. 8(b) shows the bode diagrams of the analytical results compared to ANSYS[†]-simulation results. The bode plot shows a very good conformance between simulation and analytical solution. One can see, that the system with airstream channels reacts as fast as a system without channels and a gap width of $d_0 = 10 \mu\text{m}$. The error between FEM-analysis and analytical solution is also small in this case. The identified mechanical system lies also in the range of the predicted solution.

Fig. 9 shows the applied weighting scheme[‡] incorporated with the closed-loop transfer functions. The weighting directly takes the plant input disturbance into account and optimizes the plant input disturbance rejection. Apart from a good tracking response of T_i , this guarantees a good disturbance rejection for both, input and output disturbances.

The time-domain measured results compared to the simulation results shows Fig. 10. It can be seen, that the practical results show a very good conformance with the simulated results. The weighting scheme also prevents the reappearance of the open-loop poles in the closed-loop transfer functions and thus, avoids a slow disturbance rejection.

[†]ANSYS is a trademark of ANSYS, Inc., Canonsburg, PA

[‡]The weights $W_w = \epsilon$, $W_d = M_d$, $W_e = (sM_s^{-1} + \omega_b)/(s + \omega_b\epsilon)$, $W_u = (s + \omega_{bt}M_t^{-1})/(\epsilon s + \omega_{bt})$ and $W_y = M_y^{-1}$ were applied for the \mathcal{H}_∞ -minimization, where $M_d = g_{max}k_g/(k_{pwm}k_u)$, $M_s = M_y = 2.5$, $M_t = 2M_d$, $\omega_b = 2\pi 200 \text{ Hz}$, $\omega_{bt} = 10\omega_b$ and $\epsilon \rightarrow 0$.

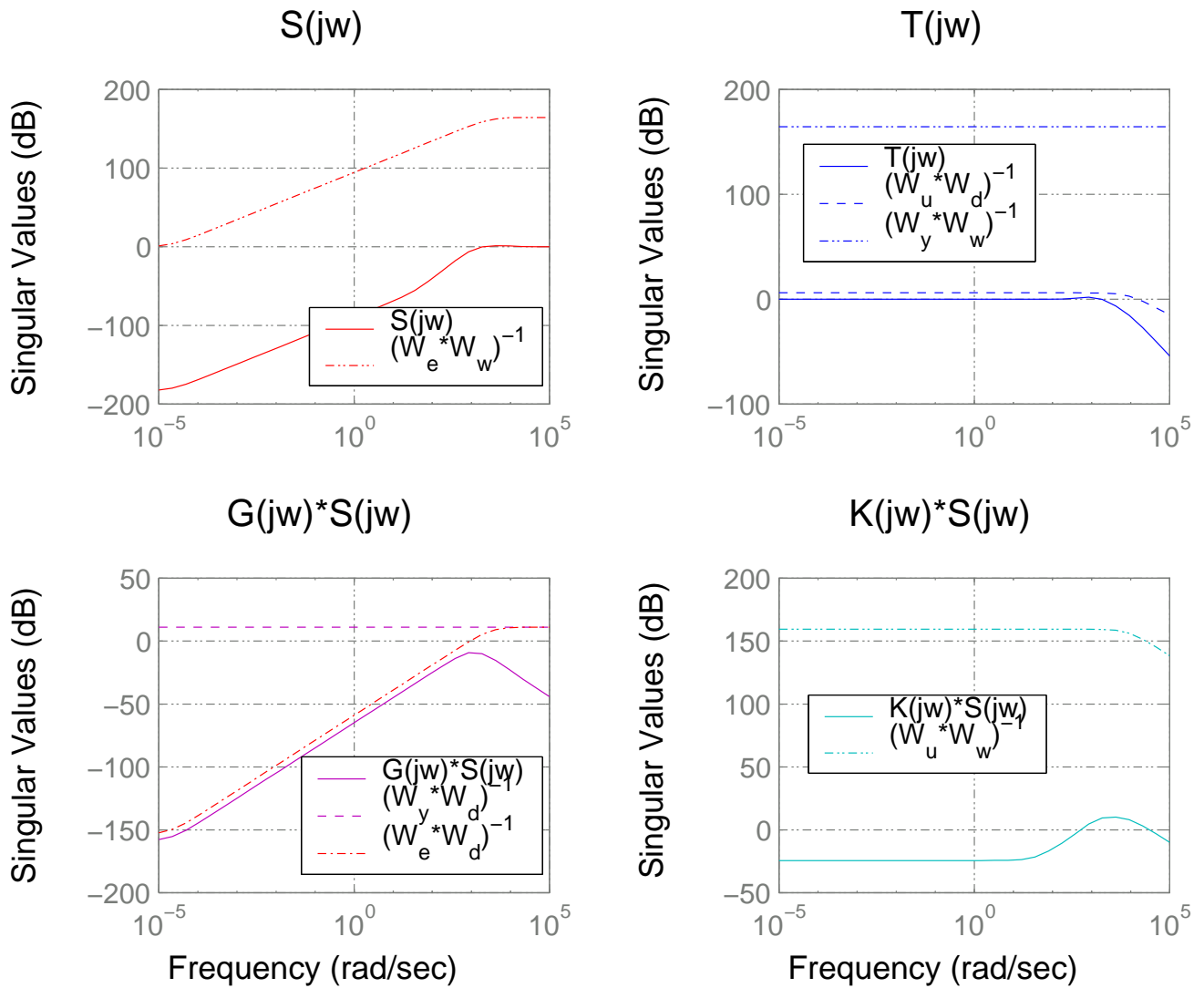
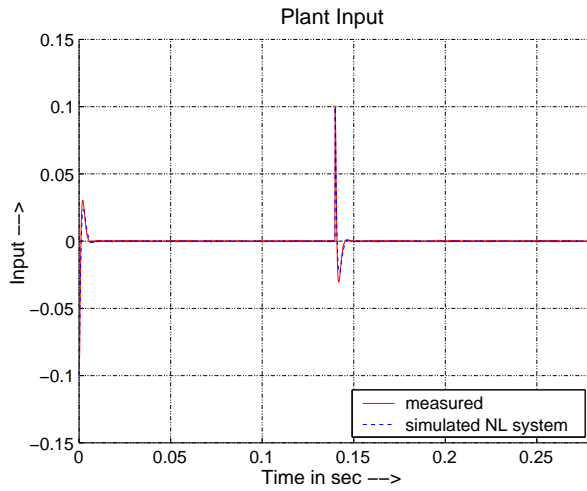


Figure 9. Applied weights incorporated with the closed-loop transfer functions at $u_b = 10$ V

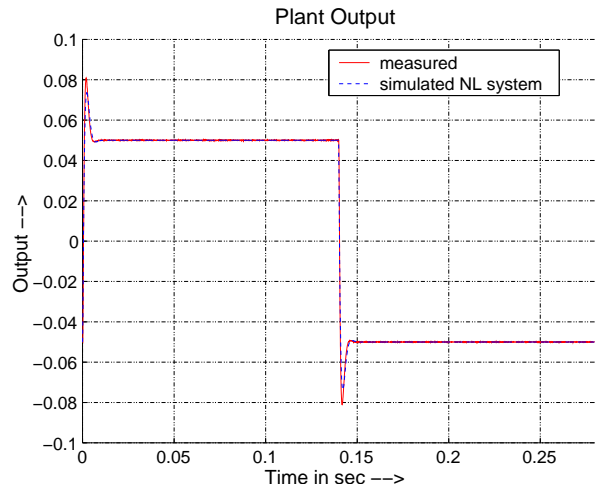
7. CONCLUSIONS

Analytical methods have been used to describe the nonlinear accelerometer system. Remarks are given on the squeeze-film analytical solution to incorporate plates with deep airstream channels to reduce the squeeze-film effect. A reduced-order LTI system for the control design was generated at the zero operating point.

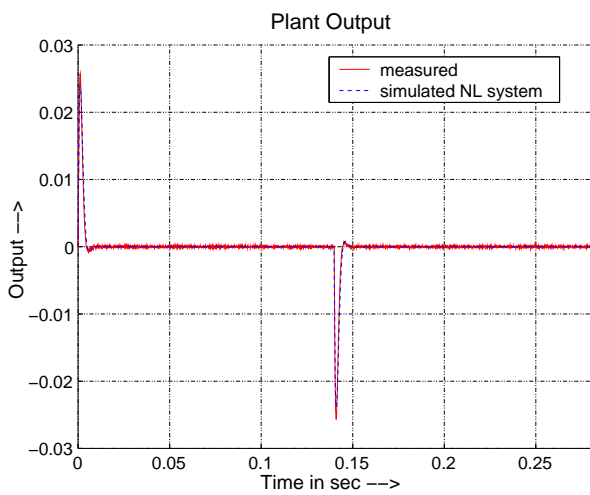
The \mathcal{H}_∞ -weighting scheme directly takes the plant input disturbance into account. This weighting avoids the open-loop pole reappearance in the closed-loop transfer function, and thus, avoids any slow



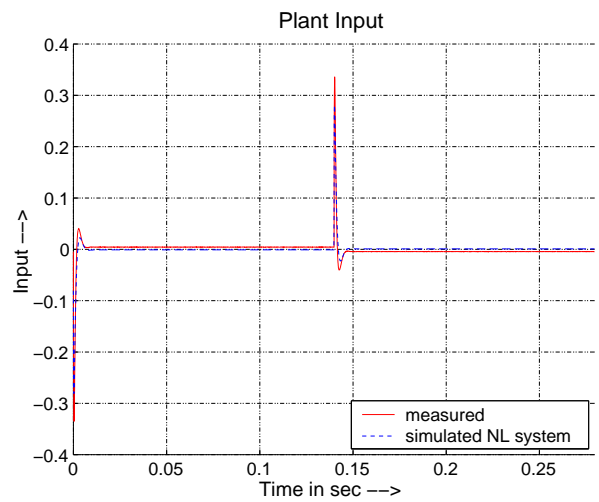
(a) Plant output disturbance response



(b) Tracking response



(c) Plant input disturbance response



(d) Control response

Figure 10. Measured and simulated step responses of the closed-loop system at $u_b = 10$ V

disturbance rejection.

The identification and control routines have been successfully applied to several sample systems. The identification routine also proves the analytical model of the mechanical and the electrostatic system, its dependence on the operating voltage and the influence of the airstream channels.

References

- 1 LU, CRIST, MARK LEMKIN, and BERNHARD E. BOSER: *A monolithic surface micromachined accelerom-*

- eter with digital output. IEEE Journal of Solid-State Circuits, 30(12):1367–1373, December 1995.
- 2 HANDTMANN, MARTIN: *Dynamische Regelung mikroelektromechanischer Systeme (MEMS) mit Hilfe kapazitiver Signalwandlung und Krafrückkoppelung*. Doktorarbeit, Technische Universität München, München, Juli 2004.
 - 3 WINE, DAVID W., MARK P. HELSEL, LORNE JENKINS, HAKAN UREY, and THOR D. OSBORN: *Performance of a biaxial mems-based scanner for microdisplay applications*. In MOTAMEDI, M. EDWARD and ROLF GOERING (editors): *MOEMS and Miniaturized Systems*, volume 4178 of *Proceedings of SPIE*, pages 186–196, Santa Clara, CA, September 2000. SPIE.
 - 4 CHEUNG, PATRICK, ROBERTO HOROWITZ, and ROGER T. HOWE: *Design, fabrication, position sensing, and control of an electrostatically-driven polysilicon microactuator*. IEEE Transactions on Magnetics, 32(1):122–128, January 1996.
 - 5 HORSLEY, DAVID A., NAIYAVUDHI WONGKOMET, ROBERTO HOROWITZ, and ALBERT P. PISANO: *Precision positioning using a microfabricated electrostatic actuator*. IEEE Transactions on Magnetics, 35(2):993–999, March 1999.
 - 6 LIAO, KE-MIN, YI-CHIH WANG, CHIH-HSIEN YEH, and RONGSHUN CHEN: *Closed-loop adaptive control for torsional micromirrors*. In EL-FATATRY, AYMAN (editor): *MOEMS and Miniaturized Systems IV*, volume 5346 of *Proceedings of SPIE*, pages 184–192, Bellingham, WA, 2004. SPIE.
 - 7 PARK, SUNGSU, ROBERTO HOROWITZ, and CHIN-WOO TAN: *Adaptive controller design of mems gyroscopes*. In *Proceedings of the 2001 IEEE Intelligent Transportation Systems*, pages 496–501, Oakland, CA, August 25–29, 2001. IEEE.
 - 8 PARK, SUNGSU and ROBERTO HOROWITZ: *Adaptive control for the conventional mode of operation of mems gyroscopes*. Journal of Microelectromechanical Systems, 12(1):101–108, February 2003.
 - 9 GAURA, E. I., N. FERREIRA, R. J. RIDER, and N. STEELE: *Closed-loop, neural network controlled accelerometer design*. In LAUDON, MATTHEW and BART ROMANOWICZ (editors): *Proceedings of the Third International Conference on Modeling and Simulation of Microsystems*, pages 513–516, San Diego, CA, March 27–29, 2000.
 - 10 SANE, HARSHAD S., NAVID YAZDI, and CARLOS MASTRANGELO: *Robust control of electrostatic torsional micromirrors using adaptive sliding-mode control*. In *Proceedings of SPIE – Photonics West 2005*, volume 5719, pages 115–126, San Jose, CA, January 22–27, 2005.
 - 11 JUNEAU, THOR, KLAUS UNTERKOFLE, TONY SELIVERSTOV, SAM ZHANG, and MICHAEL JUDY: *Dual-axis optical mirror positioning using a nonlinear closed-loop controller*. In *Transducers: International Conference on Solid State Sensors, Actuators and Microsystems*, volume 1 & 2, pages 560–563, Boston, MA, June 2003. IEEE.
 - 12 WINKLER, JOHANNES und HORST AURICH: *Technische Mechanik*. Nachschlagebücher für Grundlagenfächer. VEB Fachbuchverlag Leipzig, 1985.
 - 13 LANGLOIS, W. E.: *Isothermal squeeze films*. Quarterly of Applied Mathematics, 20(2):131–150, 1962.

- 14 GRIFFIN, W. S., H. H. RICHARDSON, and S. YAMANAMI: *A study of fluid squeeze-film damping*. Journal of Basic Engineering, Transactions of the ASME, 88:451–456, 1966.
- 15 WOLFRAM, HEIKO, RALF SCHMIEDEL, KARLA HILLER, TORSTEN AURICH, WOLFGANG GÜNTHER, STEFFEN KURTH, JAN MEHNER, WOLFRAM DÖTZEL, and THOMAS GESSNER: *Model building, control design and practical implementation of a high precision, high dynamical mems acceleration sensor*. In *Proc. of SPIE*, Sevilla, Spain, May 09–11, 2005. SPIE.
- 16 UCHIDA, NORIO, KIYOTAKA UCHIMARU, MINORU YONEZAWA, and MASAYUKI SEKIMURA: *Damping of micro electrostatic torsion mirror caused by air-film viscosity*. In *International Conference on Micro Electro Mechanical Systems*, pages 449–454, Miyazaki, Japan, January 23–27, 2000. IEEE.
- 17 WOLFRAM, HEIKO, RALF SCHMIEDEL, KARLA HILLER, THORSTEN AURICH, WOLFGANG GÜNTHER, WOLFRAM DÖTZEL und THOMAS GESSNER: *Modellierung, Reglerentwurf und Praxistest eines hochdynamischen MEMS-Präzisionsbeschleunigungssensors*. In: *5. GMM/ITG/GI-Workshop Multi-Nature Systems*, Seiten 33–40, Dresden, 18. Februar 2005. Fraunhofer-Institut für Integrierte Schaltungen.
- 18 VAN OVERSCHEE, PETER and BART DE MOOR: *Subspace Identification for Linear Systems – Theory - Implementation - Applications*. Kluwer Academic Publishers, Boston, London, Dordrecht, 1996.
- 19 ZHOU, KEMIN and JOHN C. DOYLE: *Essentials of Robust Control*. Prentice Hall, Upper Saddle River, NJ, 1998.

Authors:

Heiko Wolfram
Chemnitz University of Technology,
Faculty of Electrical Engineering and Information Technology
Reichenhainer Str. 70
09126 Chemnitz, Germany
Telephone: +49 (0)371/531-3274
Fax: +49 (0)371/531-3259
E-mail: <heiko.wolfram@etit.tu-chemnitz.de>

Ralf Schmiedel
Chemnitz University of Technology,
Faculty of Electrical Engineering and Information Technology
Reichenhainer Str. 70
09126 Chemnitz, Germany
Telephone: +49 (0)371/531-3253
Fax: +49 (0)371/531-3131
E-mail: <ralf.schmiedel@zfm.tu-chemnitz.de>

Torsten Aurich
GEMAC – Gesellschaft für Mikroelektronikanwendungen Chemnitz m.b.H.
Zwickauer Str. 227
09116 Chemnitz, Germany
Telephone: +49 (0)371/3377-305
Fax: +49 (0)371/3377-272
E-mail: <aurich@gemac-chemnitz.de>

Jan Mehner
Fraunhofer Institute for Reliability and Microintegration
Reichenhainer Str. 88
09126 Chemnitz, Germany
Telephone: +49 (0)371/5397-924
Fax: +49 (0)371/5397-310
E-mail: <jan.mehner@che.izm.fraunhofer.de>

Thomas Geßner
Chemnitz University of Technology,
Faculty of Electrical Engineering and Information Technology
Reichenhainer Str. 70
09126 Chemnitz, Germany
Telephone: +49 (0)371/531-3130
Fax: +49 (0)371/531-3131
E-mail: <thomas.gessner@zfm.tu-chemnitz.de>

Wolfram Dötzel
Chemnitz University of Technology,
Faculty of Electrical Engineering and Information Technology
Reichenhainer Str. 70
09126 Chemnitz, Germany
Telephone: +49 (0)371/531-3264
Fax: +49 (0)371/531-3259
E-mail: <wolfram.doetzel@etit.tu-chemnitz.de>